Diffusive transport of light in sea ice

H. J. Trodahl, R. G. Buckley, and S. Brown

A new experimental technique has been developed and tested in McMurdo Sound, Antarctica for the *in situ* measurement of the diffusive transport of light through sea ice. A weakly divergent monochromatic light source is placed on the surface of the ice, and the emergent radiation field is measured at both the top and bottom surfaces. The spatial and angular distribution of the emergent radiance, combined with the results of Monte Carlo simulations, has given a simple and direct measurement of the light scattering length, inhomogeneity, and anisotropy in this very complex material.

I. Introduction

The scattering and absorption of sunlight by sea ice have a considerable effect on the energy balance of the earth's polar regions, ultimately asserting control over meterological, oceanographic, and biological systems. Despite this importance, there have been relatively few attempts to perform optical characterization measurements on sea ice, although a number of measurements of sunlight levels in and under the ice have been reported.[1-6] Grenfell and co-workers[7-15] have compared the experimental results with those predicted by idealized models of the ice, which include depth-dependent bubble and brine distributions, but to our knowledge no attempt has been made to derive scattering and absorption parameters directly from experimental data. In this paper we report the successful implementation of a simple measurement technique and an analysis scheme that extracts depth-dependent optical parameters from the data.

Our experimental technique[16] centers on an artificial monochromatic source placed on the surface of the ice and the measurement of the transmitted and backscattered light as a function of the source–detector separation. By employing two detectors with different angular responses in the transmission experiment, it is possible to characterize the angular distribution of the transmitted light and estimate the net transmitted flux. The results of the transmission, backscattering, and angular dependence experiments have been compared with the results of a series of Monte Carlo simulations[17-19] to identify the important characteristics of the interaction of light with this complex material. We demonstrate that with this technique it is possible to study the effects of layering and of anisotropic scattering on the propagation of light through sea ice.

II. Experimental

A. Instrumental

The experimental technique is illustrated in Fig. 1. The source delivered radiative power to a small spot on the surface of the ice, while the detectors measured the radiative intensities emerging from both top and bottom ice surfaces as a function of the horizontal component ρ of the source–detector separation. The entire measurement was necessarily performed in the presence of sunlight; thus the source was chopped at a 27-Hz frequency, and the detector signal was processed with a phase-locked amplifier. The important new aspect of our experiment is the measurement of the ρ dependence of the emerging radiation, for this carries information about the depth dependence and anisotropy of the scattering length.

The source consists of a 50-W quartz–halogen lamp whose element was imaged with an $f/0.77$ 38.5-mm focal length lens onto a chopper-filter plane using a magnification of 10. After passing through the chopper and a filter slide position, the light traveled a further 25 mm to the ice surface, entering the surface at normal incidence and with a spot size of ~30 mm. Wavelength selection was accomplished by placing in the filter position Schott interference filters with a

J. Trodahl is with Victoria University of Wellington, Physics Department, Private Bag, Wellington, New Zealand; when this work was done both the other authors were with Department of Scientific & Industrial Research, Physics & Engineering Laboratory, Private Bag, Lower Hutt, New Zealand; S. Brown is now with Sidney Sussex College, Physics Department, Cambridge, U.K.

Received 17 December 1986.
0003-6935/87/153005-07$02.00/0.

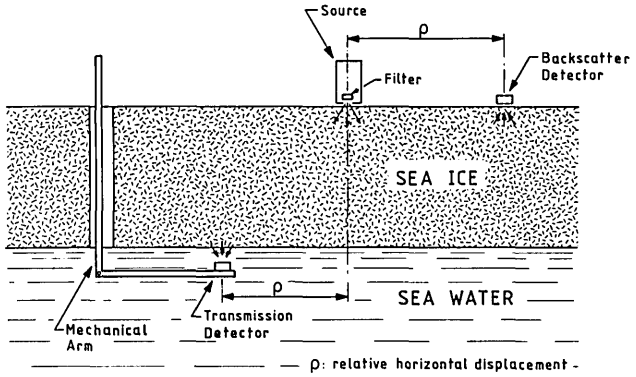

Fig. 1. Schematic diagram of the source and detector layout for both the transmission and backscattering measurement. The flux is measured as a function of the horizontal component of the source–detector separation ρ by moving the two elements on the surface of the ice.

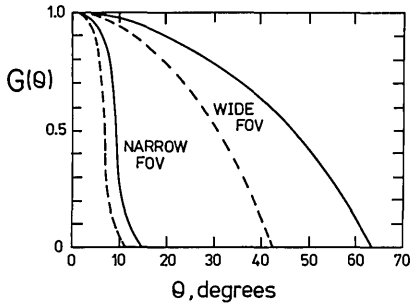

Fig. 2. Angular response functions of the detectors (solid) and transformed to represent the underwater response (dashed).

passband width of 50 nm centered on every 50 nm from 400 to 1000 nm.

The detecting element was an EG&G HUV 4000B Silicon photodiode of 100-mm^2 area in a package that included an amplifier. To obtain information about the angular distribution of the emergent radiation, we mounted detectors in two configurations with differing fields of view. The first had the detector immediately behind a 40-mm diam glass window, while in the second the detector was placed at the focus of an $f/0.74$ 29.5-mm focal length lens. The angular response functions of the two configurations were measured in the laboratory by rotating the detector housing about an axis passing through the window in the presence of a small constant source. These response functions and their transformation for underwater use are shown in Fig. 2.

The two detectors were positioned underwater using a simple aluminum arm hinged 1.4 m from the detectors and when in position viewed directly the bottom surface of the ice. The distance from the detectors to the ice could be adjusted by raising or lowering the entire assembly. In practice this distance was held as small as possible, typically <50 mm.

For the backscattering experiments a downward facing wide field-of-view detector was placed directly on the ice and sampled a 50-mm diam spot on the ice surface. Backscattered sunlight was naturally very strong at the surface; thus it was found necessary to introduce a 1% neutral density filter in place of the glass window to prevent saturation of the detector. The physical sizes of the source and detector prevented backscattering data at points closer than 100 mm from the source.

B. Measurement and Data Reduction Scheme

To normalize the emergent radiance it was necessary to obtain a measure of the power P_λ emitted by the source. This was determined by placing the detectors ~5 m in front of the source and measuring the resulting detector signal v_λ at points (x,y) in the plane perpendicular to the optical axis. A measure in detector units of the net source power is then the integral of the distribution, i.e.,

$$\int v_\lambda(x,y)dxdy \equiv v_{0\lambda}(0,0)A. \tag{1}$$

In practice, we assumed that the angular source distribution was the same at all wavelengths and measured the entire distribution and thus A in white light only. $v_{0\lambda}(0,0)$ was measured through each filter and with both detector assemblies. To prevent detector saturation during this procedure, it was necessary to use a neutral density filter of nominally 10^3 attenuation. The spectral transmission of the neutral density filter was determined in the laboratory.

In terms of this normalization method, the relative emergent radiance (I_λ/P_λ) integrated over the angular response of the detector is given by

$$R_\lambda(\rho) \equiv \frac{v_\lambda(\rho)}{Av_{0\lambda}(0,0)} = \frac{1}{P_\lambda}\int_{2\pi} d\Omega G_\lambda(\theta)I_\lambda(\rho,\theta,\phi), \tag{2}$$

where $v_{0\lambda}(0,0)$ is the normalization signal described above, $v_\lambda(\rho)$ is the signal strength when the detector is in position ρ, and $G_\lambda(\theta)$ is the angular response function of the detector normalized to unity at $\theta = 0$. The wavelength-dependent detector sensitivity drops out in the ratio. The radiance is written as a function of the polar and azimuthal angles (θ,ϕ) of the detector, which in practice always had the polar axis lying normal to the ice surface. Note that if the radiance shows azimuthal symmetry about this axis, Eq. (2) simplifies to

$$R_\lambda(\rho) \equiv \frac{2\pi}{P_\lambda}\int_0^1 I_\lambda(\theta)G_\lambda(\theta)d(\cos\theta). \tag{2a}$$

This angular averaged radiance can be compared to the expression for the total relative emergent flux:

$$F_\lambda(\rho) = \frac{2\pi}{P_\lambda}\int_0^1 I_\lambda(\theta)\cos\theta d(\cos\theta), \tag{3}$$

in terms of which the net fraction of transmitted radiation is

$$T_\lambda = 2\pi \int F_\lambda(\rho)\rho d\rho. \tag{4}$$

As noted above, two detectors with quite different angular response functions were used in the transmission experiment, yielding different angular averages of the radiance and resulting in information about the angular distribution of the emergent radiance. As will

be argued, this permitted us to estimate the relative emergent flux $F_\lambda(\rho)$ and the net transmission T_λ from the measured radiance $R_\lambda(\rho)$.

In principle the net fraction of backscattered light (the albedo) could have been estimated by a similar precedure, but this was prevented by the lack of backscattering data at small ρ.

III. Results

The purpose of this paper is to demonstrate the utility of the measurement scheme; thus we include in this section only enough results to achieve that purpose. A more complete set of results, and a discussion of their implication for ice physics, is the subject of another paper.

The instrument has been used to study first year sea ice near Tent Island in McMurdo Sound, Antarctica. During the measurements in Nov. 1985 the ice in the area was 1.5–1.7 m thick. Data were collected at three sites (*A*,*B*,*C*). Light snow covers of (25,15) mm at sites (*A*,*B*) were cleared before measurements were taken. Site *C* was free of snow.

A. Angular Dependence of Emergent Radiation

One of the most notable results is that at all wavelengths and for all ρ the ratio of the integrated transmitted radiance $R_\lambda(\rho)$ [see Eq. (2)] for the narrow field-of-view (FOV) detector to that for the wide FOV detector was between 0.09 and 0.14. The large range quoted for this ratio is a result of (1) uncertainties in the field calibration, particularly for the narrow FOV detector, and (2) a ±10% scatter in the measured ratio. There was no systematic variation of the measured ratio with wavelength or source–detector displacement. The implication is that the angular distribution of the radiance $I_\lambda(\theta)$ is largely determined by wavelength independent scattering in the ice and that the angular distribution retained no memory of the source position. More important, the size of the ratio implies a very strongly peaked angular distribution. To demonstrate this, we note that under isotropic radiation with the radiance I_λ independent of θ, the ratio generated by Eq. (2), using the angular response functions of Fig. 2, is 0.055. Clearly the narrow FOV detector receives more light than it would in an isotropic radiation field. The weakly peaked distribution emerging from an isotropic scattering medium[18] predicts a ratio that is only marginally larger at 0.059.

In the absence of further theoretical guidance concerning the radiance angular distribution, we modeled it with several functional forms, estimating the distribution widths by fitting to the measured narrow-to-wide FOV ratio. The halfwidths determined in this way are in the 20–35° range with the major variation caused by uncertainties in the experimental ratio rather than by the functional forms assumed.

The confirmation that such a narrow distribution is realistic was provided by making dc measurements of sunlight radiance while lowering the detector support arm. These showed a very rapid decrease at what were still relatively small angles ($\theta < 45°$).

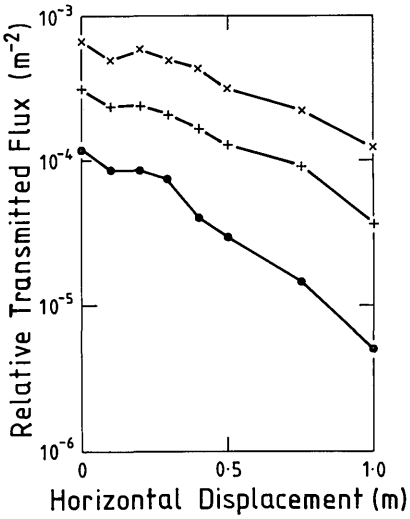

Fig. 3. Plot of the relative transmitted flux against source–detector displacement at site *C*. This plot illustrates the falloff in flux with increasing source–detector displacement and the narrowing of the distribution with increasing wavelength for wavelengths >600 nm: ×, 500 nm; +, 650 nm; ●, 700 nm.

An important use of the angular information is in providing a guide to estimating the net transmitted flux from our data. In the strongly peaked radiance distributions that satisfactorily fit the narrow-to-wide FOV ratios, the wide-angle detector measures between 70 and 95% of the transmitted flux. Thus the following equations may be quoted for the relative transmitted flux $F_\lambda(\rho)$:

$$F_\lambda \approx \frac{1.15 v_\lambda(\rho)}{A v_{0\lambda}(0,0)} \tag{5}$$

for the wide FOV data and

$$F_\lambda \approx \frac{12 v_\lambda(\rho)}{A v_{0\lambda}(0,0)} \tag{6}$$

for the narrow FOV data. We estimate the accuracy of expression (5) to 15% and (6) to 25%, based on measured variations in the ratio of the narrow-to-wide angle detector signals. To make direct comparisons between data from the two detectors and the Monte Carlo simulations discussed below, we present the remainder of our results in terms of relative transmitted flux given by the above expressions.

B. Emergent Profiles $F_\lambda(\rho)$

In Fig. 3 are typical plots of the relative transmitted flux vs source–detector separation, illustrating the falloff in flux over a distance of the same order as the ice thickness. In addition to the wavelength dependence of the net transmission, there is a clear narrowing of the distribution $F_\lambda(\rho)$ as the wavelength rises above 600 nm. By performing the integral in Eq. (4) the total transmission for all sites can be calculated, as displayed in Fig. 4.

Backscatterig data for site *C* are shown in Fig. 5. In contrast to the transmission experiment a measurable signal was obtained at all wavelengths, but because of

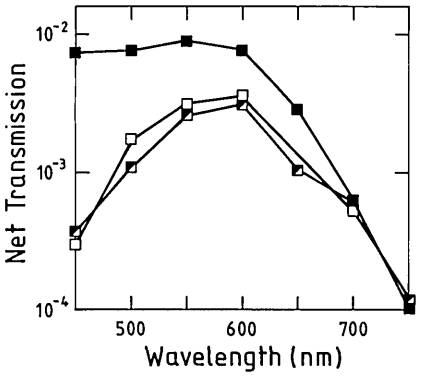

Fig. 4. Total transmission T_λ plotted against wavelength at all three experimental sites illustrating the differences between sites *A*, □; *B*, ◪; *C*, ■.

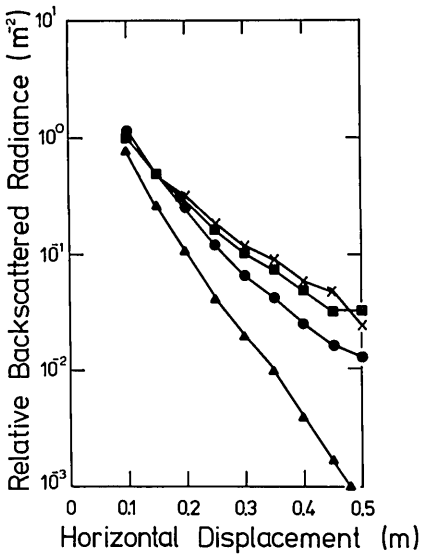

Fig. 5. Backscattered flux against source–detector separations at site *C*: ×, 500 nm; ■, 600 nm; ●, 700 nm; ▲, 800 nm.

the size of the source and detector housings, data could not be collected for $\rho < 100$ mm.

It is important to recognize that there are uncertainties in the results associated with inhomogeneities in the ice. Locations were chosen free of large scale disturbances such as old floe boundaries, cracks, or pressure ridges. Nonetheless, sea ice is a very inhomogeneous material, showing structure at many scale lengths. They are not expected to have large effects on the bulk transmission process because light passing from the source to the detector is scattered over and thus samples a large volume of ice. However, at the two end points, the source and detector, the light passes through specific small regions, and consequently if these regions are atypical, they exert an exaggerated influence on the results. (This is the source of the kink seen in the data in Fig. 3 at $\rho = 0.1$ m.) The effect was studied by repeating measurements while moving the source and detector along different radial lines and at adjacent sites. It is estimated that the individual data points represent the average characteristics of the ice at any particular site to a reliability of ~10%.

IV. Data Interpretation

Although our measurements provide a more detailed characterization of the ice than is possible with uniformly illuminated ice, there is still too little information to permit a complete determination of the variation with depth of scattering center density, phase function, and anisotropy. We, therefore, take an empirical approach and compare our results to models containing simple forms of inhomogeneity and anisotropy. With this approach, we have been able to identify the aspects of the scattering that are most important in determining the transfer of radiation in the bulk of the ice. Although we are guided in this process by observations made directly on ice cores, we have made no attempt to make first principal estimates of the scattering and absorption characteristics of the ice.

For simplicity, we characterize the scattering by a parameter δ, the scattering length, the distance in which the total momentum of a burst of photons falls to e^{-1} of its initial value. For isotropic scatterers with a total cross section σ and occurring with density n

$$\delta = (n\sigma)^{-1}. \tag{7}$$

In contrast, for the predominantly forward scattering expected from bubbles or brine inclusions in ice, the momentum transfer in one scattering event is reduced by $(1 - \cos\gamma)$, where γ is the average scattering angle. As a result, the scattering length is increased to[18]

$$\delta = [n\sigma(1 - \cos\gamma)]^{-1}. \tag{8}$$

For detailed predictions of the transmitted and backscattered profiles, we relied primarily on a Monte Carlo simulation similar to that of Groenhuis *et al.*,[19] a choice made because of the ease with which a depth-dependent scattering length could be modeled. Details of the modeling and the results are reported elsewhere,[17] and we give here only a brief summary of the results of comparing the data to Monte Carlo calculations.

A. Detailed Modeling at Site *C*

We performed detailed modeling only for the ice at site *C*, where the absence of a strongly disordered top layer (frozen grease ice) simplified the modeling. However, even at this site there was evidence of a very thin (a few centimeters) layer of ice with a high density of bubbles, and we did not try to take account of this layer directly in the Monte Carlo calculations. The major effect of this layer would be to randomize the photon directions and scatter some fraction of the source beam back out of the ice, thus reducing the power that enters the bulk. In principle there would be evidence of this backscattering in the results, but the lack of data for small source–detector separation removes the evidence. Consequently, we chose to leave the transmission α of this top surface layer as a fitted parameter.

The backscattered radiance was successfully fitted by a series of models, both with and without a depth dependence to the scattering length. In view of the ease with which the fit could be achieved, we have concentrated on homogeneous models (i.e., constant

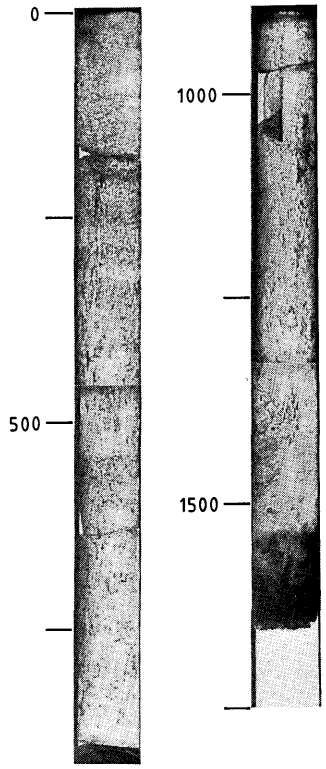

Fig. 6. Vertical core of sea ice from site *B*. Clearly seen is the granular surface layer (upper left) that gives way to the columnar structure in the bulk. The dark band at the base of the ice (lower right) is due to algae. The numbers down the left side of the core give the depth in millimeters.

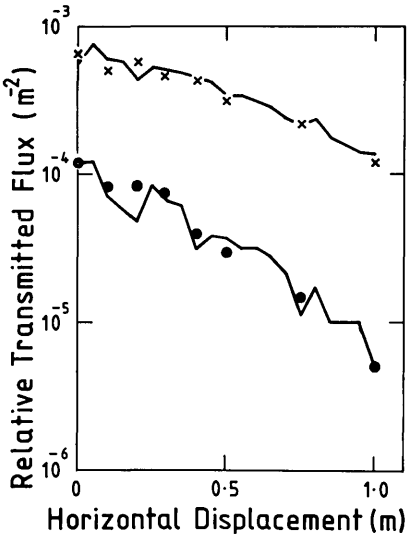

Fig. 7. Transmitted flux at site *C* and Monte Carlo results for a two-layered model but with anisotropic scattering in the second layer. The optical parameters are $\eta = 0.1\ m^{-1}$, δ (top layer) = 0.06 m, δ_0 = 0.2 m and δ_1 = 0.1 m at 500 nm (×) and $\eta = 0.7\ m^{-1}$, δ (top layer) = 0.06 m, δ_0 = 0.2 m, and δ_1 = 0.1 m at 700 nm (●).

δ), for which diffusion equation solutions are also available.[19] The diffusion and Monte Carlo models are in agreement.[17] Detailed fits were performed using the absorption coefficients η corresponding to the pure ice values at 500 nm ($0.05\ m^{-1}$) and 700 nm ($0.7\ m^{-1}$)[11] to find that the scattering length implied by the measurements at these wavelengths was 0.055 ± 0.005 m. This must be regarded as an average over the thickness of the ice probed by the backscattering measurement, over the top few hundred millimeters. The transmission α of the surface layer required to obtain a fit was 0.5 ± 0.2.

Transmission profiles could not be fit to any homogeneous model, since even when the absorption coefficient was allowed to exceed that of pure ice, the combinations of η and δ that yielded acceptable fits to backscattered data gave a too strongly attenuated transmission. Guided by the typical core structure shown in Fig. 6, we adopted layered models with a scattering length in the top 0.2–0.5 m differing from the remainder. These yielded acceptable fits to the backscattered profile and to the net transmission, but the predicted transmission profiles remained significantly wider than the measured profiles.

Our most successful models were based on a lower layer ($\geq$1 m thick) with anisotropic scattering chosen to reflect the predominantly vertical defect structure in sea ice (see Fig. 6). The scattering was modeled by a distribution of oriented surfaces which scatter at a rate of $(1/\delta_1)$ for each unit length of horizontal travel embedded in a background of normal (unoriented) centers that scatter at a rate of $(1/\delta_0)$. The scattering length is then dependent on the angle θ that a ray makes to the vertical as

$$\frac{1}{\delta} = \frac{1}{\delta_0} + \frac{\sin\theta}{\delta_1}.$$

The scattering lengths δ_v for vertical ($\theta = 0$) and δ_h for horizontal ($\theta = \pi/2$) rays are then δ_0 and $\delta_0\delta_1/(\delta_0 + \delta_1)$, respectively.

The range of parameters that give acceptable fits to our data is not large (±25%), and we show in Fig. 7 the best fits at 500 and 700 nm. This most successful model had 0.5 m of isotropic ice ($\delta_v = \delta_h$) with a 0.06-m scattering length followed by 1.1 m of ice with δ_0 and δ_1 of 0.2 and 0.1 m, respectively. Thus the horizontal scattering length is 0.067 in the anisotropic layer. The absorption coefficients, treated as fitting parameters, were $(0.1,0.7)\ m^{-1}$ for (500,700) nm, slightly larger than the pure ice literature values[11] of $(0.05,0.5)\ m^{-1}$. The transmission of the surface required to fit the backscattered radiance was again (0.5 ± 0.2). The transmission fit, however, required a further attenuation of (0.17,0.5) at the two wavelengths (500,700) nm. The excess attenuation is due to the color selective absorption in the algae layer seen in Fig. 6.

Another prediction of the anisotropic scattering model is that the angular distribution of the radiation emerging from the bottom surface of the ice is peaked around the vertical. The halfwidth of this angular distribution in the best fit model is $30° \pm 5°$, in reasonable agreement with the distribution inferred from the measurements with the wide- and narrow-FOV detectors.

The average distance between scattering events can be calculated by using Eq. (8) and the phase function

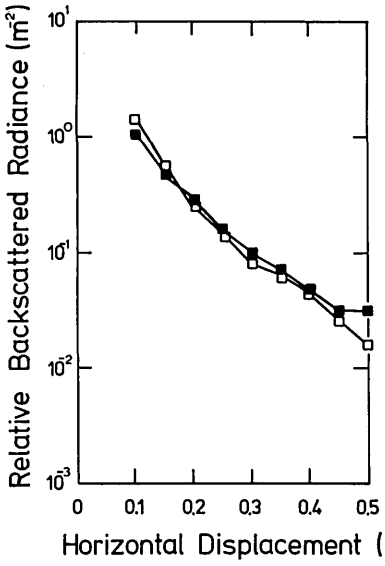

Fig. 8. Enhanced backscattered flux at small displacements at site B (□) over that measured at site C (■) and the reverse at large displacements.

NaCl ice.[8] The distance of 3–6 mm is in agreement with the brine channel separation seen in core photographs (Fig. 6).

B. Sites *A* and *B*

The optical characteristics of the ice at sites A and B differed significantly from those at site C. Most striking is that the transmission at A and B was a factor of ~5 smaller than at C, and the 500-nm absorption band was deeper (Fig. 4). The reduced transmission at 500 nm was not accompanied by a reduction in the width of the distribution $F_\lambda(\rho)$ as was observed from data above 600 nm. Since an increased absorption in the bulk of the ice reduces this width [as well as the magnitude of $F_\lambda(0)$], it follows that the 500-nm absorption occurs in a thin layer within the ice. It is clearly attributable to the algae layer in platelet ice near the bottom surface. This layer could be seen in ice cores (see Fig. 6) and was thicker at sites A and B than at site C. Algae also contributed at least part of the decreasing transmission outside this band, for it is known they show a finite absorption right across the visible.[20]

The backscattered data from site B identify another source of the reduced transmission. As illustrated in Fig. 8, at large source–detector separations these lie a factor of between 1.5 and 2 below those at site C, while at minimum separation the site B intensities are larger. The major part of the backscattered power at all sites lies inside the minimum separation of 100 mm; thus it is clear that the albedo is larger at site B. We ascribe this to the layer of disordered frozen grease ice at this site. As an estimate of the reduction in the surface layer transmission, we take the ratio in the backscattered radiance at larger separation, where the largest contribution is from light that has entered the bulk of the ice. The surface transmission at site B is then ~70% of that at site C.

V. Conclusions

We have studied light diffusion and absorption in sea ice by measuring the backscattered and transmitted radiation fields from a small monochromatic source placed on the ice surface. The facility to measure as a function of source–detector separation permits a more detailed study than is possible with the more commonly employed technique of relying on uniform solar illumination. In particular, our simple *in situ* measurements interpreted with the aid of extensive Monte Carlo simulations have revealed

(1) a scattering length of 0.055 m near the ice surface;

(2) a longer and anisotropic scattering length through the bulk of the ice;

(3) the presence of attenuation of light at both the top and bottom surfaces;

(4) a wavelength dependence of the bottom surface attenuation that follows the expected absorption by algae.

Measurements were conducted at three sites with differing apparent ice structure. It was found that the optical character of the bulk of the ice was the same at all three sites with significant differences only in their surface attenuations.

We acknowledge the logistic support of the Antarctic Division of DSIR, the technical help of personnel at PEL and David Gilmour of Victoria University of Wellington, and Arnold Heine for assistance in the field.

References

1. V. V. Bogorodskii and E. S. Volodin, "Attenuation of Collimated Light Beams in Layers of Snow and Sea Ice," Sov. Phys. Dokl. **27**, 235 (1982).
2. H. Davis and R. H. Munis, "Effect of Salinity on the Optical Extinction of Sea Ice at 6328Å," CRREL Research Report 308 (1973).
3. B. Ya. Gaitskhoki, "Spectral Transmission of Snow and Some Ice Varieties," in *The Physics of Ice*, V. V. Bogorodskii, Ed. (Israel Program for Scientific Translations, Jerusalem, 1971), p. 44.
4. J. W. Lane, "Optical Properties of Salt Ice," J. Glaciol. **73**, 363 (1975).
5. C. W. Thomas, "On the Transfer of Visible Radiation Through Sea Ice and Snow," J. Glaciol. **4**, 481 (1963).
6. G. E. Weller, "Radiation Diffusion in Antarctic Ice Media," Nature London **221**, 355 (1969).
7. T. C. Grenfell, "The Effects of Ice Thickness on the Exchange of Solar Radiation over the Polar Oceans," J. Glaciol. **22**, 305 (1979).
8. T. C. Grenfell and D. Hedrick, "Scattering of Visible and Near Infrared Radiation by NaCl Ice and Glacier Ice," Cold Reg. Sci. Technol. **8**, 119 (1983).
9. T. C. Grenfell, "A Theoretical Model of the Optical Properties of Sea Ice in the Visible and Near Infrared," J. Geophys. Res. **88**, 9723 (1983).
10. T. C. Grenfell and G. A. Maykut, "The Optical Properties of Ice and Snow in the Arctic Basin," J. Glaciol. **18**, 445 (1977).
11. T. C. Grenfell and D. K. Perovich, "Radiation Absorption Coefficients of Polycrystalline Ice from 400–1400 nm," J. Geophys. Res. **86**, 7447 (1981).
12. G. A. Maykut and T. C. Grenfell, "The Spectral Distribution of Light Beneath First-Year Sea Ice in the Arctic Ocean," Limnol. Oceanogr. **20**, 554 (1975).

13. D. K. Perovich and T. C. Grenfell, "Laboratory Studies of the Optical Properties of Young Sea Ice," J. Glaciol. **27,** 331 (1981).
14. D. K. Perovich and T. C. Grenfell, "A Theoretical Model of Radiative Transfer in Young Sea Ice," J. Glaciol. **28,** 341 (1982).
15. R. R. Roulet, G. A. Maykut, and T. C. Grenfell, "Spectrophotometers for the Measurement of Light in Polar Ice and Snow," Appl. Opt. **13,** 1652 (1974).
16. R. G. Buckley, H. J. Trodahl, and P. J. Langhorne, "Scattering and Absorption of Visible Light in Sea Ice from Transmission and Backscattering Measurements," Physics and Engineering Laboratory Report 951 (1986).
17. S. A. Brown, R. G. Buckley, and H. J. Trodahl, "Modeling of Optical Measurements on Sea Ice," Physics and Engineering Laboratory Report 948 (1986).
18. H. C. van de Hulst, *Multiple Light Scattering Tables, Formulas, and Applications, Vol. 1* (Academic, New York, 1980).
19. R. A. J. Groenhuis, H. A. Ferwerda, and J. J. Ten Bosch, "Scattering and Absorption of Turbid Materials Determined from Reflection Measurements. 1: Theory," Appl. Opt. **22,** 2456 (1983).
20. J. T. O. Kirk, *Light and Photosynthesis in Aquatic Ecosystems* (Cambridge U. P., Cambridge, 1983).

CALL FOR PAPERS

on a special issue in Applied Optics

OPTICAL PATTERN RECOGNITION AND ASSOCIATIVE RETRIEVAL PROCESS

Recently the techniques of optical pattern recognition and associative retrieval process have attracted the attention and interests of many optical processors because there are increasing needs of real-time tracking for machine/robotic vision in high-level automation systems. Also, recognition and neural-type association are indispensable for future artificially intelligent "super computers". Therefore, we would like to devote a special issue of *Applied Optics* to this important topic during the year 1988. The content of the papers called for should address, but not be limited to, the following subjects:

Optical System Design

* preprocessing
* postprocessing
* data reduction
* information extraction
* distortion-free design
* dynamic range compression
* multivariate image processing
* associate-retrieval implementation

Optical Matched Filter Design

* adaptability
* programmability
* efficiency and storage capacity
* Fourier vs. non-Fourier transform
* rotation, scale, aspects, and illumination invariance

Hybrid Systems, Optical Components, and Devices

* spatial light modulators
* holographic optical elements
* nonlinear photorefractive crystals
* computer-generated holograms
* two-wave and four-wave mixing schemes
* optical-digital interface
* new architectures and algorithms
* hybrid associative-retrieval systems

Please mail manuscript before November 30, 1987 to Dr. Hua-Kuang Liu, M/S 198-231, Jet Propulsion Laboratory, California Institute of Technology, 4800 Oak Grove Dr. Pasadena, CA 91109.